Sensors and Actuators B 226 (2016) 266–272

Contents lists available at ScienceDirect

Sensors and Actuators B: Chemical

journal homepage: www.elsevier.com/locate/snb

Au nanoparticle-functionalized 3D SnO_2 microstructures for high performance gas sensor

Jing Guo [a], Jun Zhang [a,b,*], Haibo Gong [a], Dianxing Ju [a], Bingqiang Cao [a,*]

[a] Laboratory of Inorganic Functional Materials, School of Materials Science and Engineering, University of Jinan, Jinan 250022, Shandong, China
[b] College of Physics, Qingdao University, Qingdao 266071, China

ARTICLE INFO

Article history:
Received 5 July 2015
Received in revised form
11 November 2015
Accepted 30 November 2015
Available online 3 December 2015

Keywords:
SnO_2
Nanostructures
Au
Sensor
High performance

ABSTRACT

Three-dimensional (3D) nanostructures of metal oxides have been widely used for gas sensor devices. In this work, 3D porous SnO_2 microstructures constructed by two-dimensional (2D) nanosheets were prepared via a simple hydrothermal process combined with subsequent annealing. Gold (Au) nanoparticles were successfully immobilized onto the surface of SnO_2 nanosheets to serve as a sensitizer by a facile solution reduction process. This novel 3D Au/SnO_2 microstructure has been investigated for gas senor and exhibits remarkably enhanced sensing performances to ethanol, e.g. high response, fast recovery time and good stability. The possible sensing mechanism is also discussed in terms of the special effect of Au functionalization.

1. Introduction

SnO_2, an important metal oxide, has been recognized as a promising semiconductor material for many applications such as gas sensors [1–3], lithium-ion batteries [4,5], electrocatalysts [6,7], supercapacitors [8,9], solar cells [10,11] and so forth. Especially, SnO_2 is widely used for gas sensors due to its excellent performance compared with other metal oxides. It could detect many different kinds of gas pollutants, toxic and combustible gases which are dangerous to both environment and humans, including NO_2 [12,13], CO [14,15], H_2S [16,17] and some organic compound gases [18,19]. Its working temperature is relatively lower compared with other metal oxide semiconductors. Hence, less power consumption is needed [20,21]. In addition, the relative high response and good stability of SnO_2 sensing material enable the gas sensor device to work with high efficiency during a long time [22].

The morphologies, structures and sizes of metal oxide materials have been proved to influence their sensing performances. Low-dimensional structures such as nanoparticles tend to aggregate to lose their large surface area and high surface reactivity when working at elevated temperatures, which will deteriorate the stability of gas sensors. In contrast, three-dimensional (3D) porous structures with enhanced structure stability will remain its sensitivity within a long time even at relative high working temperature. Generally, 3D microstructures can be assembled by 0D nanocrystals [23], 1D nanorods [24] and 2D nanosheets [25]. The special 2D structure like nanosheet or nanoplate has a lager specific surface area compared with others. For surface-controlled gas sensing material, increasing the contact area between material and target gases will provide more surface active sites for the sensing reactions. In addition, the porous structure of the sensing materials can improve the gas diffusion within the sensing layer, hence enhancing the sensor properties [26,27]. Therefore, this special 3D microstructure would expect better performance compared with bulk material. The large inner space among the nanosheets will provide facile transport pathways or channels, which makes the diffusion of gas molecules more easily.

Considering 3D nanostructures are good candidates for gas sensing materials, it is important to further optimize the device performances for practical applications. Typically, noble metals such as Au, Pt and Pd, despite of their high cost, have been chosen as an efficient "sensitizer" to improve the performance of gas sensing materials [28–30]. For instance, porous α-Fe_2O_3 decorated by Au nanoparticles [31] exhibited highly enhanced performance to ethanol compared with pristine Fe_2O_3 particles. Both Au-loaded ZnO hollow nanospheres nanospheres [32] and Au@ZnO yolk-shell structures [30] demonstrated obvious improvement in response compared to pure ZnO. Au-functionalized SnO_2 hollow spheres [33,34] are also reported to exhibit superior sensitivity to

* Corresponding authors. Tel.: +86 531 8973 6292; fax: +86 531 8276 4453.
E-mail addresses: mse_zhangj@ujn.edu.cn (J. Zhang), mse_caobq@ujn.edu.cn (B. Cao).

http://dx.doi.org/10.1016/j.snb.2015.11.140
0925-4005/

the test gases. The above investigations indicate noble metal particles truly exhibit superiorities in improving the performance of gas sensing materials.

In this contribution, 3D SnO_2 microstructures assembled with 2D porous nanosheets were synthesized and further used as a framework to load Au nanoparticles. The obtained 3D Au/SnO_2 microstructures were characterized in detail and their gas sensing performance was investigated. Due to the advantageous synergic effect of the 3D microstructures composed of porous nanosheets and the unique property of Au nanoparticles, the Au/SnO_2 sensor displayed superior performance over pristine SnO_2 in terms of high response, fast response–recovery time and good stability. Gas sensing mechanism for the Au/SnO_2 sensing material is also discussed.

2. Experimental

2.1. Chemicals

All chemical reagents, including $SnCl_2{\cdot}2H_2O$, NaOH, hexadecyltrimethylammonium bromide (CTAB), lysine ($C_6H_{14}N_2O_2$), $NaBH_4$, $HAuCl_4{\cdot}4H_2O$ were of analytical grade and were used as-received without any further purification. Deionized water (resistance higher than 18.2 MΩ cm) was used during the experiment.

2.2. Synthesis of 3D SnO_2 microstructures

SnO_2 microstructures were synthesized by a hydrothermal method. In a typical synthesis process, 0.46 g $SnCl_2{\cdot}2H_2O$ was dissolved in 20 mL deionized water and 0.33 g NaOH and 0.74 g CTAB dispersed in 20 mL deionized water. After stirring for about half an hour, the two solutions were mixed together under stirring until changing into a transparent solution. Then the mixture was transferred into a Teflon-lined stainless steel autoclave of 50 mL capacity. The autoclave was sealed and kept at 120 °C for 12 h. After reaction, the autoclave was cooled down naturally. The original precipitate was centrifuged and washed with ethanol and deionized water, respectively. Finally the yellow powder was obtained after 12 h dehydration at 80 °C. The calcination was performed in a muffle furnace at 500 °C for 2 h.

2.3. Synthesis of Au/SnO_2 hybrids

The synthesis of Au/SnO_2 hybrids followed a similar reported method [28]. 0.1 g SnO_2, 1.5 mL (0.01 M) $HAuCl_4$ and 1.5 mL (0.01 M) lysine was dispersed into 15 mL deionized water under stirring. 15 minutes later, 0.2 mL (0.1 M) $NaBH_4$ was introduced into the mixture. After vigorous stirring for another 20 min, the purple solution was centrifuged with deionized water and ethanol, respectively. After drying at 80 °C overnight, the sample was calcined at 300 °C for 30 min to obtain Au/SnO_2 hybrid materials.

2.4. Characterizations and gas sensing measurement

Structure and phase identification were measured by power X-ray diffraction (XRD) using a Bruker diffractrometer (D8-Advance) with Cu $K\alpha$ radiation of 1.5418 Å. The morphologies of SnO_2 and Au/SnO_2 microstructures were observed by a scanning electron microscope (SEM, Quanta FEG 250) and high resolution transmission electron microscope (HRTEM, JEM-200CX). The elemental composition is tested by energy-dispersive X-ray spectroscopy (EDS) attached to SEM.

The gas sensor was fabricated as descripted previously in our former paper [22]. A small amount of powder sample was ground in an agate mortar with several drops of deionized water to make the powder into a homogeneous paste. Then the slurry was coated on an aluminum tube (4 mm in length and 1 mm in diameter) to form a thin film with uniform thickness. Two Au electrodes and four Pt wires were positioned on both ends of the tube and a Ni–Cr alloy coil working as a heater through the tube to control operating temperature by tuning the heating voltage. For comparison, two series of gas sensors were fabricated using pristine SnO_2 and Au/SnO_2, respectively. The sensors were aged for 3 days on the measurement system before gas sensing test.

Gas sensing tests were performed with a WS-60A gas sensing measurement system (Winsen Electronics, China) at a relative humidity of 20%. This is a static system using atmospheric air as the reference and dilute gas. The sensors are placed into a transparent testing chamber whose volume is 20 L. Target gas with calculated amount is introduced into the test chamber by a syringe. Two electric fans installed in the chamber are used to make test gas homogeneous. The sensor response S is defined as the ratio of R_a/R_g where R_a and R_g are the electrical resistance of the sensor in air and target gas, respectively.

3. Results and discussion

3.1. Characterization

The phase and crystal structure of the samples have been identified by XRD, and Fig. 1 shows the XRD patterns of different as-prepared powders. Clearly, the sample obtained from hydrothermal exhibits obvious diffraction peaks of both SnO (JCPDS No. 77-2296) and SnO_2 (JCPDS No. 41-1445) in Fig. 1(a). The crystallite size of the sample is 4.84 nm calculated by using Scherer equation based on (1 1 0) peak. After calcination for 2 h at 500 °C, the sample changes into SnO_2 completely and all the diffraction peaks match well with the typical tetragonal rutile structure of SnO_2, as shown in Fig. 1(b). The crystallite size of the 3D SnO_2 materials is calculated to be 20.5 nm by Scherer equation based on (1 1 0) peak. The calcination improved the crystallization and also promotes the growth of grains during the annealing process. After loading Au nanoparticles onto the nanosheets (Fig. 1c), three typical diffraction peaks indexed to metallic Au (JCPDS No. 89-3697) [2] was observed and. The average grain size of Au nanoparticle was calculated to be 7.06 nm by Scherrer equation based on (2 0 0) peaks. The relatively weak diffraction peaks of Au indicate a small amount and a nanometer size in the hybrid materials.

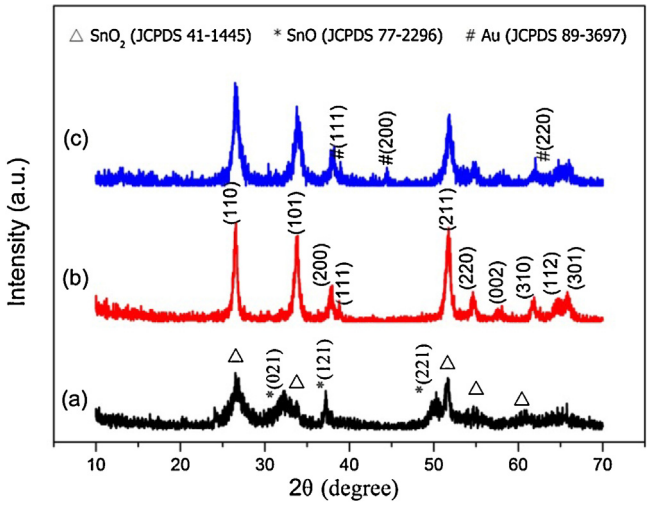

Fig. 1. XRD patterns of (a) sample obtained from hydrothermal process; (b) SnO_2 obtained after calcination; (c) Au/SnO_2 hybrids.

The morphology and structure of SnO_2 and Au/SnO_2 were characterized with SEM. Fig. 2(a) and (b), are SEM images of the sample obtained from hydrothermal process. The chemical reaction occurs as follows under alkaline condition.

$$SnCl_2 + OH^- = SnCl(OH) \quad (1)$$

$$SnCl(OH) + OH^- = Sn(OH)_2 \quad (2)$$

$$Sn(OH)_2 = SnO + H_2O \quad (3)$$

$$SnO + 1/2O_2 = SnO_2 \quad (4)$$

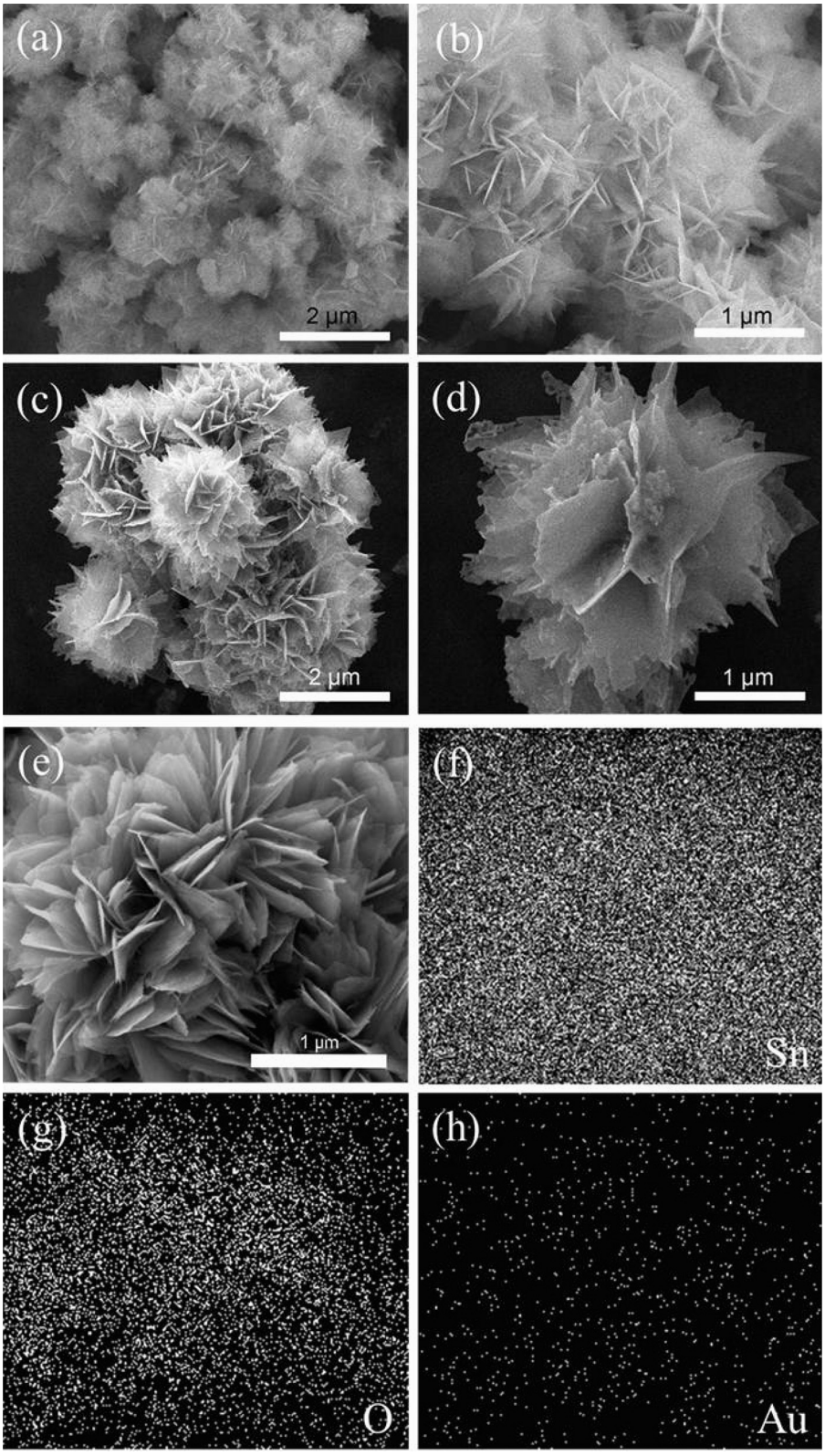

Fig. 2. SEM of (a and b) sample obtained from hydrothermal process; (c and d) SnO_2 microstructure after calcination; (e) Au/SnO_2 microstructures; (f–h) distribution of elements corresponding to (e).

Reactions (1)–(3) and part of (4) took place under high temperature provided by the autoclave. So the powder after hydrothermal reaction includes both SnO and SnO_2 as shown in the XRD pattern. After calcination at elevated temperature, SnO was oxidized into SnO_2 completely as proved in Fig. 1(b). During this process, many pores with different sizes form at both the edges and surface of nanosheets, endowing the nanosheets with a porous structure, which makes the material surface quite rough as shown in Fig. 2(c) and (d). The 3D SnO_2 microstructure has a large surface area of 62.5 m^2/g by BET [22]. Fig. 2(e) is the SEM of Au/SnO_2. The hybrid materials also maintain the 3D microstructure composed of uniform nanosheets. The existence of Au nanoparticles on the SnO_2 nanosheets is further proved by EDS. Fig. 2(f), (g) and (h) show the distribution of elements (Sn, O and Au) corresponding to Fig. 2(e). From Fig. 2(h), it is clearly seen that Au nanoparticles are uniformly distributed on the nanosheets. The relative content of Au nanoparticles in the hybrids is 0.39 wt.% determined by the EDS characterization.

To further study the SnO_2 2D microstructure and distribution of Au nanoparticles, Au/SnO_2 was characterized with TEM. As shown in Fig. 3(a), Au nanoparticles with diameter ranging from 5 to 10 nm distribute uniformly on the nanosheets. Fig. 3(b) is a typical HRTEM of the Au/SnO_2 nanosheet. A distinct set of lattice fringes of SnO_2 were revealed and the length between the adjacent lattice planes is estimated to be 0.33 nm, which is in good agreement with the distance between the (1 1 0) planes [35]. In the center of this HRTEM picture is a typical Au nanoparticle with dark contrast and the lattice spacing of 0.24 nm is consistent with the (1 1 1) planes of Au [36]. Furthermore, pores with irregular shapes in the nanosheet can also be seen, which is potentially beneficial for the diffusion and transport of gas molecules in the sensors.

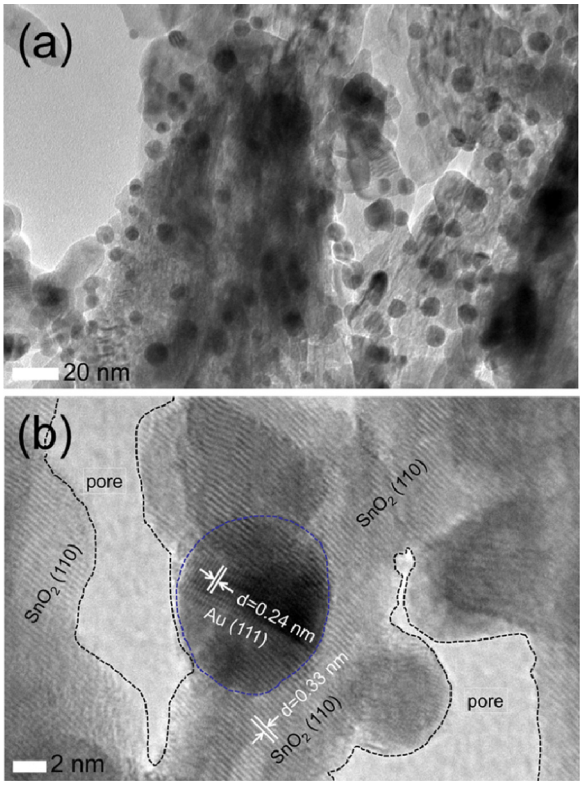

Fig. 3. (a) TEM image, (b) HRTEM image for the as-synthesized Au/SnO_2 microstructures composed of nanosheets with pores.

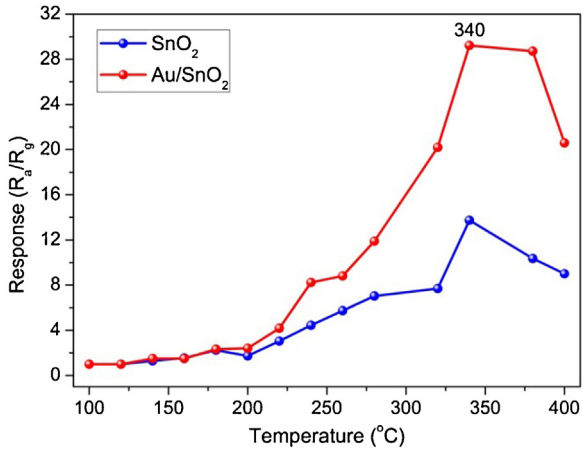

Fig. 4. Response of SnO_2 and Au/SnO_2 to 150 ppm ethanol at various temperatures (100–400 °C).

3.2. Gas sensing performance

Inspired by the 3D porous Au/SnO_2 hybrid microstructures and catalytic effect of Au nanoparticles, the gas sensing performance of the Au/SnO_2 hybrids was evaluated.

Working temperature usually has a great influence on gas sensing performance [37], as it influences the adsorption and desorption process of oxygen molecules. Control tests to 150 ppm ethanol were performed from 100 to 400 °C in order to determine the optimum operating temperature of the sensors. As shown in Fig. 4, the gas response of both SnO_2 and Au/SnO_2 sensors increases with the increasing temperature and reaches the maximum at about 340 °C. However, the Au/SnO_2 sensor exhibits a much higher response than pure SnO_2, which should be ascribed to the loading of Au nanoparticles, and will be discussed later in detail. The response of Au/SnO_2 to 150 ppm ethanol (29.3) is actually 2 times higher than that of pristine SnO_2 (13.7) at 340 °C.

Fig. 5 shows the dynamic response–recovery curves of the two sensors to ethanol of different concentrations (5, 20, 50, 100, 200, 500 and 1000 ppm) at 340 °C and the inset illustrations are gas sensors corresponding to SnO_2 and Au/SnO_2 microstructures. The gray SnO_2 changes into purple indicating the successful decoration of Au onto SnO_2 microstructures. The response amplitude of both sensors increases with the increasing of ethanol concentration. The

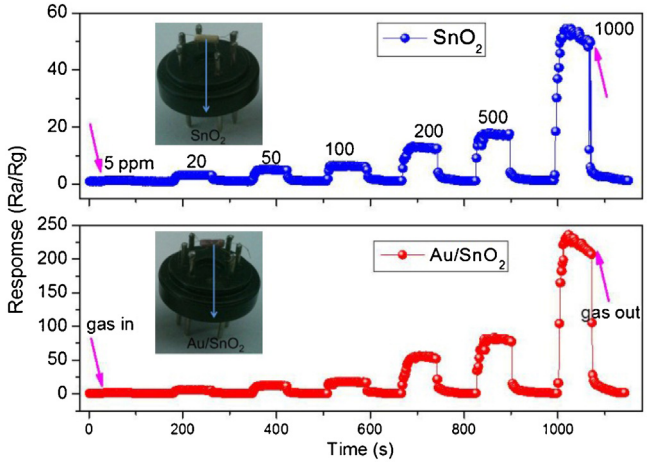

Fig. 5. Real-time response of SnO_2 and Au/SnO_2 to different ethanol concentrations (5, 20, 50, 100, 200, 500 and 1000 ppm) at 340 °C and the inset illustrations are gas sensors corresponding to SnO_2 and Au/SnO_2 microstructures.

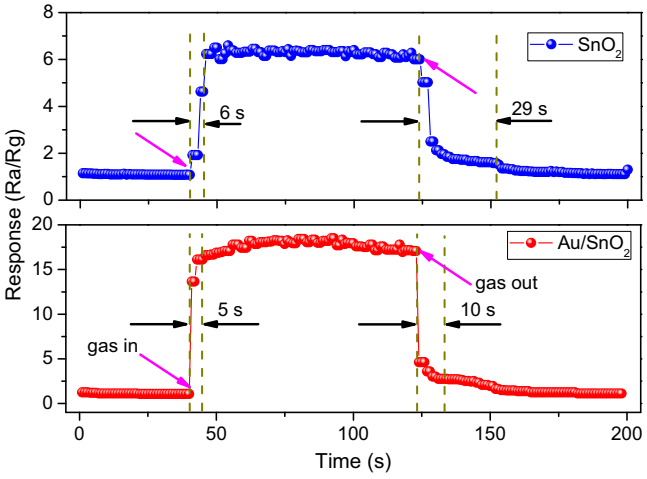

Fig. 6. Dynamic response–recovery curve of two sensors to 100 ppm ethanol at 340 °C.

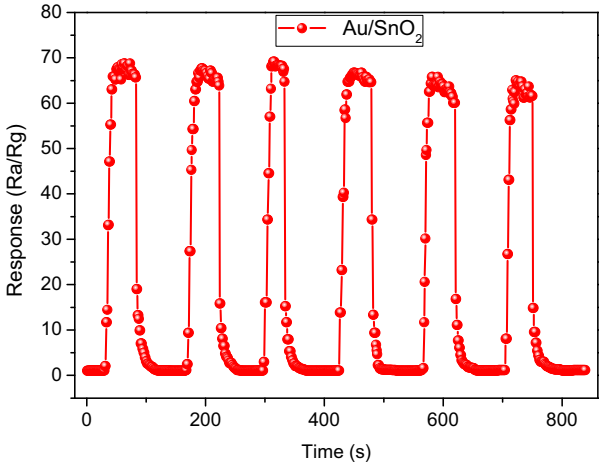

Fig. 7. Response of Au/SnO_2 gas sensors to 500 ppm ethanol at 340 °C.

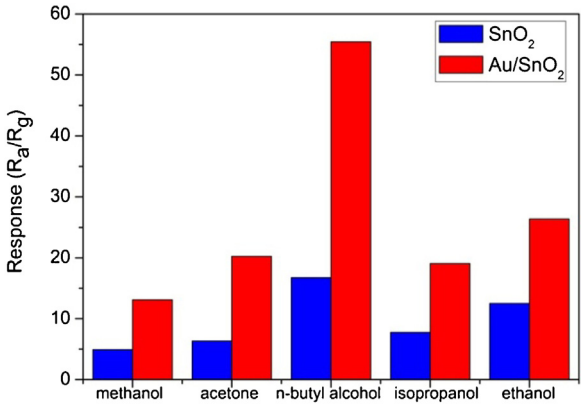

Fig. 8. Response of SnO_2 and Au/SnO_2 to 150 ppm various gases at 340 °C.

corresponding response of Au/SnO_2 hybrids is much larger than that of pure SnO_2, which manifests the outstanding performance of the hybrid materials due to the functionalization of Au nanoparticles.

Fig. 6 is the real-time dynamic response curves to 100 ppm ethanol of the SnO_2 and Au/SnO_2 sensors at 340 °C. Evidently, the Au/SnO_2 sensor has much higher response (18), which is nearly three times higher than that of SnO_2 (6.3). Besides, response–recovery time is also an important parameter that should be considered in order to meet the application of gas sensors. Fig. 6 is the real-time response curves to 100 ppm ethanol of the SnO_2 and Au/SnO_2 sensors. Herein, we define the response and recovery time as the time required to reach 90% of the total change. As shown in Fig. 6, the response time of SnO_2 and Au/SnO_2 sensors is estimated to be 6 s and 5 s, and the recovery time is 29 s and 10 s, respectively. To evaluate the sensing performance of as-prepared Au/SnO_2 hybrid nanosheets, a comparison between our result and the literatures is summarized in Table 1. As can be seen, the SnO_2 nanofibers synthesized by Zhang [38] has fast response and recovery, and the specific value toward 10 ppm ethanol was ~13 s and ~13.9 s. Usually, recovery time will be longer if the target gas stands at a high concentration level [39]. That is, if high concentration of ethanol was tested, it would take more time for the sensor to achieve balance to in the desorption process. A diversity of SnO_2 sensors measured at different preset conditions are compared in Table 1. The fast response of this Au/SnO_2 sensor might be attributed to the microstructures assembled by porous nanosheets, and, at the same time, Au nanoparticles truly exhibit significant catalysis effect on accelerating the recovery process [28].

Fig. 7 plots the real-time response of the Au/SnO_2 gas sensor to 500 ppm ethanol with 6 cycles at 340 °C, which exhibits good repeatability with fast response and recovery. Therefore, the existence of Au nanoparticles not only increases the response, reduces response–recovery time but retain good stability during the gas sensing test.

The selectivity of the SnO_2 and Au/SnO_2 microstructures was further investigated with different kinds of volatilize organic gases, including methanol, ethanol, acetone, isopropanol and *n*-butanol at 150 ppm, as shown in Fig. 8. By comparison, it can be seen that Au/SnO_2 has much larger response to all the test gases (13.3, 26.5, 20.3, 19.0 and 55.5) than SnO_2 (5.0, 12.6, 6.4, 7.8 and 16.6) to methanol, ethanol, acetone, isopropanol and *n*-butanol, respectively. All the responses of Au/SnO_2 are more than 2 times higher than that of SnO_2. Besides, both sensors manifest the highest response to *n*-butanol, which indicates a potential selectivity to *n*-butanol. The selectivity of gas sensors depends on the chemical properties of test gases, as well as the sensing materials. Herein, the higher responses to *n*-butanol may be because *n*-butanol is more active to lose electrons on oxidation by chemisorbed oxygen species.

Table 1
Performance comparison of various SnO_2-based gas sensors to ethanol.

Sample	Concentrations of ethanol (ppm)	Temperature (°C)	Response	Response/recovery time (s)
SnO_2 nanofibers [38]	10	330	~4.5	13/13.9
SnO_2 nanowires [39]	100	400	10.5	2/136
La_2O_3–SnO_2 nanowires [39]	100	400	57.3	1/110
Hollow SnO_2 nanofiber [40]	100	200	35.02	86/14
Hierarchical SnO_2 [41]	100	300	24.1	6/70
Au/SnO_2 nanobelts [42]	100	100	194.77%	67/58
Au/SnO_2 microstructures in this work	100	340	18	5/10

3.3. Gas sensing mechanism

SnO_2 is a typical n-type semiconductor and its conductivity is highly influenced by the surface depletion layer, which is characteristic of the surface-controlled type of sensing material, especially for nanostructures. Therefore, the mechanism of SnO_2 gas sensor is based on the resistance change before and after exposing to the target gas. When the SnO_2 gas sensor is exposed to air, oxygen molecules will be absorbed on the material surface and extract electrons from the conduction band and form ionized oxygen species (O_2^-, O^- and O^{2-}) [43]. As a consequence, an electron depletion layer is formed due to the lack of electrons at the surface, as shown in Fig. 9(a). The sensor resistance then stands at a relative high level. When the gas sensor is exposed to reducing gas e.g. ethanol, the oxygen species would react with the gas molecules and release electrons back to the conduction band. The thickness of the electron depletion layer decrease and, therefore, the sensor resistances of the material decrease as shown in Fig. 9(b).

Compared with SnO_2 gas sensor, the Au/SnO_2 composite microstructures demonstrated significantly improved gas sensing performance. The enhancement of gas sensing properties of Au/SnO_2 microstructures can be explained by the following two aspects [44,45]. One is the chemical catalytic effect from Au nanoparticle. Au nanoparticles can increase the adsorption of oxygen molecules through spillover effect [46–49], resulting in both fast and more prolific electron capture and release. In addition, it is reported that nano-Schottky junctions would form between metal and semiconductors [50]. It results in the electron transfer from semiconductor to noble Au nanoparticles. Both factors result in additional nanometer electron depletion regions on the nanosheets surfaces. The electron depletion regions at this moment are much thicker, and R_a of the Au/SnO_2 sensor resistance is becoming much larger than that of pristine SnO_2 sensor, as compared with Fig. 9(a) and (c). When reductive ethanol is introduced, it reacts with the adsorbed oxygen species and decreases the thickness of the depletion layer. Due to the spillover effect from Au nanoparticle on SnO_2, more oxygen species will be generated to react with gas molecules. As a result, both factors will decrease the thickness of the depletion layer. Compared with SnO_2, Au/SnO_2 will lower the height of the nano-Schottky barrier and increase the conductance [50,51], as compared in Fig. 9(b) and (d). Thus, the nano-Schottky barrier junctions act as a signal amplifier to greatly improve the gas sensing response. This proposed sensing mechanism by constructing Schottky contacts may also apply to design more chemiresistive semiconductor sensors.

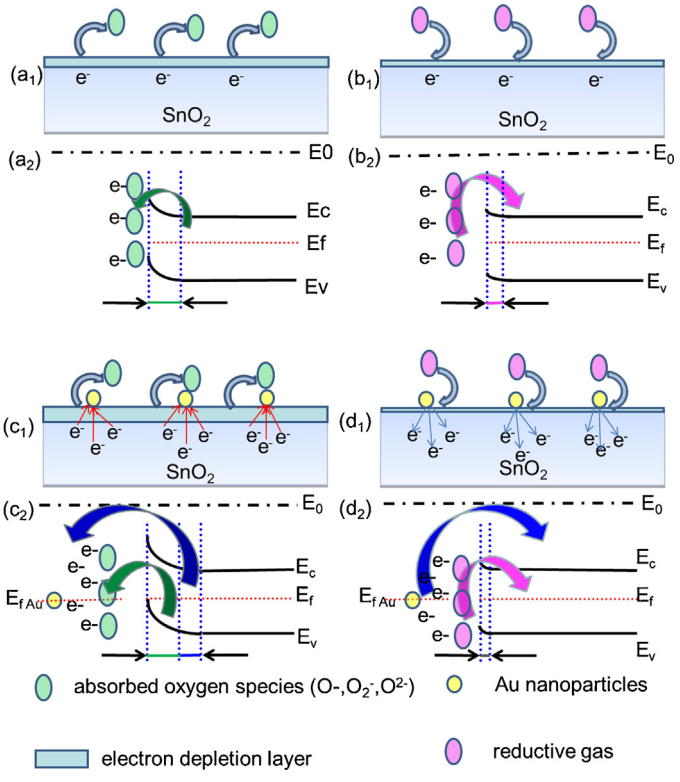

Fig. 9. Schematic gas sensing mechanism and energy band change of SnO_2 and Au/SnO_2 nanosheet.

4. Conclusions

In summary, a high performance gas sensor based on Au-functionalized 3D SnO_2 microstructures was fabricated and demonstrated superior gas sensing performance in comparison to pristine SnO_2. The 3D SnO_2 microstructures were synthesized by a facile hydrothermal process combining with subsequent annealing. The successful decoration of Au nanoparticles onto SnO_2 nanosheets plays a crucial role in improving the ethanol sensing properties. The Au/SnO_2 sensor manifests high response, fast response–recovery time and good repeatability resulting from the combination of 3D porous structure with unique properties of Au nanoparticles. The superior sensing features indicate the present Au/SnO_2 microstructures are promising for gas sensor.

Acknowledgments

This work is supported by NSFC (11174112, 51472110) and Shandong Provincial Science Foundation (ZR2015BQ006, JQ201214, 2014ZRB019JP, ZR2014JL045). The research programs (213021A) from Ministry of Education, China, are also acknowledged.

References

[1] J. Zhang, J. Guo, H.Y. Xu, B.Q. Cao, Reactive-template fabrication of porous SnO_2 nanotubes and their remarkable gas-sensing performance, ACS Appl. Mater. Interfaces 5 (2013) 7893–7898.
[2] J.M. Ma, J. Zhang, S.R. Wang, Q.H. Wang, L.F. Jiao, J.Q. Yang, X.C. Duan, Z.F. Liu, J.B. Lian, W.J. Zheng, Superior gas-sensing and lithium-storage performance SnO_2 nanocrystals synthesized by hydrothermal method, CrystEngComm 13 (2011) 6077–6081.
[3] B. Wang, L.F. Zhu, Y.H. Yang, N.S. Xu, G.W. Yang, Fabrication of a SnO_2 nanowire gas sensor and sensor performance for hydrogen, J. Phys. Chem. C 112 (2008) 6643–6647.
[4] X.W. Lou, Y. Wang, C.L. Yuan, J.Y. Lee, L.A. Archer, Template-free synthesis of SnO_2 hollow nanostructures with high lithium storage capacity, Adv. Mater. 18 (2006) 2325–2329.
[5] W.M. Zhang, J.S. Hu, Y.G. Guo, S.F. Zheng, L.S. Zhong, W.G. Song, L.J. Wan, Tin-nanoparticles encapsulated in elastic hollow carbon spheres for high-performance anode material in lithium-ion batteries, Adv. Mater. 20 (2008) 1160–1165.
[6] L.H. Jiang, G.Q. Sun, Z.H. Zhou, S.G. Sun, Q. Wang, S.Y. Yan, H.Q. Li, J. Tian, J.S. Guo, B. Zhou, Size-controllable synthesis of monodispersed SnO_2 nanoparticles and application in electrocatalysts, J. Phys. Chem. B 109 (2005) 8774–8778.
[7] Q.R. Zhao, Y. Gao, X. Bai, C.Z. Wu, Y. Xie, Facile synthesis of SnO_2 hollow nanospheres and applications in gas sensors and electrocatalysts, Eur. J. Inorg. Chem. 8 (2006) 1643–1648.
[8] F.H. Li, J.F. Song, H.F. Yang, S.Y. Gan, Q.X. Zhang, D.X. Han, A. Ivaska, L. Niu, One-step synthesis of graphene/SnO_2 nanocomposites and its application in electrochemical supercapacitors, Nanotechnology 20 (2009) 455602–455607.
[9] S.L. Kuo, N.L. Wu, Composite supercapacitor containing tin oxide and electroplated ruthenium oxide, Electrochem. Solid State Lett. 6 (2003) A85–A87.
[10] S. Gubbala, V. Chakrapani, V. Kumar, M.K. Sunkara, Band-edge engineered hybrid structures for dye-sensitized solar cells based on SnO_2 nanowires, Adv. Funct. Mater. 18 (2008) 2411–2418.
[11] H.J. Snaith, C. Ducati, SnO_2-based dye-sensitized hybrid solar cells exhibiting near unity absorbed photon-to-electron conversion efficiency, Nano Lett. 10 (2010) 1259–1265.

[12] J. Zhang, S.R. Wang, Y.M. Wang, Y. Wang, B.L. Zhu, H.J. Xia, X.Z. Guo, S.M. Zhang, W.P. Huang, S.H. Wu, NO_2 sensing performance of SnO_2 hollow-sphere sensor, Sens. Actuators, B: Chem. 135 (2009) 610–617.
[13] S.W. Choi, A. Katoch, G.J. Sun, P. Wu, S.S. Kim, NO_2-sensing performance of SnO_2 microrods by functionalization of Ag nanoparticles, J. Mater. Chem. C 1 (2013) 2834–2841.
[14] W. Zeng, M.Y. Wu, Y.Q. Li, S.F. Wu, Hydrothermal synthesis of different SnO_2 nanosheets with CO gas sensing properties, J. Mater. Sci.—Mater. Electron. 24 (2013) 3701–3706.
[15] K. Wang, T.Y. Zhao, G. Lian, Q.Q. Yu, C.H. Luan, Q.L. Wang, D.L. Cui, Room temperature CO sensor fabricated from Pt-loaded SnO_2 porous nanosolid, Sens. Actuators, B: Chem. 184 (2013) 33–39.
[16] W. Luo, Q.Y. Fu, D.X. Zhou, J.F. Deng, H. Liu, G.P. Yan, A surface acoustic wave H_2S gas sensor employing nanocrystalline SnO_2 thin film, Sens. Actuators, B: Chem. 176 (2013) 746–752.
[17] L.J. ping, Y. Wang, X.G. Gao, Q. Ma, L. Wang, J.H. Han, H_2S sensing properties of the SnO_2-based thin films, Sens. Actuators, B: Chem. 65 (2000) 111–113.
[18] D.J. Liu, T.M. Liu, H.J. Zhang, C.L. Lv, W. Zeng, J.Y. Zhang, Gas sensing mechanism and properties of Ce-doped SnO_2 sensors for volatile organic compounds, Mater. Sci. Semicond. Process. 15 (2012) 438–444.
[19] J.R. Huang, X.J. Xu, C.P. Gu, W.Z. Wang, B.Y. Geng, Y.F. Sun, J.H. Liu, Effective VOCs gas sensor based on porous SnO_2 microcubes prepared via spontaneous phase segregation, Sens. Actuators, B: Chem. 173 (2012) 599–606.
[20] A. Sharma, M. Tomar, V. Gupta, A low temperature operated NO_2 gas sensor based on TeO_2/SnO_2 pn heterointerface, Sens. Actuators, B: Chem. 176 (2012) 875–883.
[21] Z.F. Dai, L. Xu, G.T. Duan, T. Li, H. Zhang, Y. Li, Y. Wang, Y. Wang, W. Cai, Fast-response, sensitivitive and low-powered chemosensors by fusing nanostructured porous thin film and IDEs-microheater chip, Sci. Rep. 3 (2013) 1–7.
[22] J. Guo, J. Zhang, D.X. Ju, H.Y. Xu, B.Q. Cao, Three-dimensional SnO_2 microstructures assembled by porous nanosheets and their superior performance for gas sensing, Powder Technol. 250 (2013) 40–45.
[23] Z.R. Li, X.L. Li, X.X. Zhang, Y.T. Qian, Hydrothermal synthesis and characterization of novel flower-like zinc-doped SnO_2 nanocrystals, J. Cryst. Growth 291 (2006) 258–261.
[24] J.Q. He, J. Yin, D. Liu, L.X. Zhang, F.S. Cai, L.J. Bie, Enhanced acetone gas-sensing performance of La_2O_3-doped flowerlike ZnO structure composed of nanorods, Sens. Actuators, B: Chem. 182 (2013) 170–175.
[25] Y. Guan, D.W. Wang, X. Zhou, P. Sun, H.Y. Wang, J. Ma, G.Y. Lu, Hydrothermal preparation and gas sensing properties of Zn-doped SnO_2 hierarchical architectures, Sens. Actuators, B: Chem. 191 (2014) 45–52.
[26] J. Zhang, S.R. Wang, M.J. Xu, Y. Wang, B.L. Zhu, S.M. Zhang, W.P. Huang, S.H. Wu, Hierarchically porous ZnO architectures for gas sensor application, Cryst. Growth Des. 9 (2009) 3532–3537.
[27] Z.H. Jing, J.H. Zhan, Fabrication and gas-sensing properties of porous ZnO nanoplates, Adv. Mater. 20 (2008) 4547–4551.
[28] J. Guo, J. Zhang, M. Zhu, D.X. Ju, H.Y. Xu, B.Q. Cao, High-performance gas sensor based on ZnO nanowires functionalized by Au nanoparticles, Sens. Actuators, B: Chem. 199 (2014) 339–345.
[29] X.H. Liu, J. Zhang, X.Z. Guo, S.R. Wang, S.H. Wu, Core–shell α-Fe_2O_3@SnO_2/Au hybrid structures and their enhanced gas sensing properties, RSC Adv. 2 (2012) 1650–1655.
[30] X. Li, X. Zhou, H. Guo, C. Wang, J. Liu, P. Sun, F. Liu, G. Lu, Design of Au@ZnO yolk-shell nanospheres with enhanced gas sensing properties, ACS Appl. Mater. Interfaces 6 (2014) 18661–18667.
[31] X.H. Liu, J. Zhang, X.Z. Guo, S.H. Wu, S.R. Wang, Porous α-Fe_2O_3 decorated by Au nanoparticles and their enhanced sensor performance, Nanotechnology 21 (2010) 095501–095508.
[32] L.L. Wang, Z. Lou, T. Fei, T. Zhang, Templating synthesis of ZnO hollow nanospheres loaded with Au nanoparticles and their enhanced gas sensing properties, J. Mater. Chem. 22 (2012) 4767–4771.
[33] J. Zhang, X.H. Liu, S.H. Wu, M.J. Xu, X.Z.S. Guo, r. Wang, Au nanoparticle-decorated porous SnO_2 hollow spheres: a new model for a chemical sensor, J. Mater. Chem. 20 (2010) 6453–6459.
[34] S.-J. Choi, M.P. Kim, S.-J. Lee, B.J. Kim, I.-D. Kim, Facile Au catalyst loading on the inner shell of hollow SnO_2 spheres using Au-decorated block copolymer sphere templates and their selective H_2S sensing characteristics, Nanoscale 6 (2014) 11898–11903.
[35] L.L. Wang, H.M. Dou, Z. Lou, T. Zhang, Encapsuled nanoreactors (Au@SnO_2): a new sensing material for chemical sensors, Nanoscale 5 (2013) 2686–2691.
[36] W.T. Chen, Y.J. Hsu, L-Cysteine-assisted growth of core-satellite ZnS–Au nanoassemblies with high photocatalytic efficiency, Langmuir 26 (2009) 5918–5925.
[37] X.H. Liu, J. Zhang, X.Z. Guo, S.H. Wu, S.R. Wang, Enhanced sensor response of Ni-doped SnO_2 hollow spheres, Sens. Actuators, B: Chem. 152 (2011) 162–167.
[38] Y. Zhang, X.L. He, J.P. Li, Z.J. Miao, F. Huang, Fabrication and ethanol-sensing properties of micro gas sensor based on electrospun SnO_2 nanofibers, Sens. Actuators, B: Chem. 132 (2008) 67–73.
[39] N. Van Hieu, H.-R. Kim, B.-K. Ju, J.-H. Lee, Enhanced performance of SnO_2 nanowires ethanol sensor by functionalizing with La_2O_3, Sens. Actuators, B: Chem. 133 (2008) 228–234.
[40] W.Q. Li, S.Y. Ma, Y.F. Li, G.J. Yang, Y.Z. Mao, J. Luo, D.J. Gengzang, X.L. Xu, S.H. Yan, Enhanced ethanol sensing performance of hollow ZnO–SnO_2 core–shell nanofibers, Sens. Actuators, B: Chem. 211 (2015) 392–402.
[41] X.M. Zhou, W.Y. Fu, H.B. Yang, Y.Y. Zhang, M.H. Li, Y.X. Li, Novel SnO_2 hierarchical nanostructures: synthesis and their gas sensing properties, Mater. Lett. 90 (2013) 53–55.
[42] C. Jin, H. Kim, S. Park, H.W. Kim, S. Lee, C. Lee, Enhanced ethanol gas sensing properties of SnO_2 nanobelts functionalized with Au, Ceram. Int. 38 (2012) 6585–6590.
[43] N. Barsan, M. Schweizer-Berberich, W. Gopel, Fundamental and practical aspects in the design of nanoscaled SnO_2 gas sensors: a status report, Fresenius J. Anal. Chem. 365 (1999) 287–304.
[44] X. Liu, Z. Chang, L. Luo, X. Lei, J. Liu, X. Sun, Sea urchin-like Ag-α-Fe_2O_3 nanocomposite microspheres: synthesis and gas sensing applications, J. Mater. Chem. 22 (2012) 7232–7238.
[45] P. Montmeat, J.-C. Marchand, R. Lalauze, J.-P. Viricelle, G. Tournier, C. Pijolat, Physico-chemical contribution of gold metallic particles to the action of oxygen on tin dioxide sensors, Sens. Actuators, B: Chem. 95 (2003) 83–89.
[46] J. Zhang, X. Liu, S. Wu, B. Cao, S. Zheng, One-pot synthesis of Au-supported ZnO nanoplates with enhanced gas sensor performance, Sens. Actuators, B: Chem. 169 (2012) 61–66.
[47] X.W. Liu, F.Y. Wang, F. Zhen, J.R. Huang, In situ growth of Au nanoparticles on the surfaces of Cu_2O nanocubes for chemical sensors with enhanced performance, RSC Adv. 2 (2012) 7647–7651.
[48] Q. Xiang, G.F. Meng, H.B. Zhao, Y. Zhang, H. Li, W.J. Ma, J.Q. Xu, Au nanoparticle modified WO_3 nanorods with their enhanced properties for photocatalysis and gas sensing, J. Phys. Chem. C 114 (2010) 2049–2055.
[49] A. Kolmakov, D.O. Klenov, Y. Lilach, S. Stemmer, M. Moskovits, Enhanced gas sensing by individual SnO_2 nanowires and nanobelts functionalized with Pd catalyst particles, Nano Lett. 5 (2005) 667–673.
[50] T. Maosong, D. Guorui, G. Dingsan, Surface modification of oxide thin film and its gas-sensing properties, Appl. Surf. Sci. 171 (2001) 226–230.
[51] S. Pokhrel, C.E. Simion, V. Quemener, N. Bârsan, U. Weimar, Investigations of conduction mechanism in Cr_2O_3 gas sensing thick films by ac impedance spectroscopy and work function changes measurements, Sens. Actuators, B: Chem. 133 (2008) 78–83.

Biographies

Jing Guo is a graduate student focusing on oxide gas sensors for master degree at University of Jinan. She was awarded a B.Sc. degree in materials science and engineering from the same university in 2012.

Jun Zhang obtained his Ph.D. degree from the Department of Chemistry, Nankai University in 2011. His research is focused on the synthesis and applications of functional nanomaterials.

Haibo Gong is a lecturer at School of Materials Science and Engineering, University of Jinan. His main research interests are the synthesis and application of semiconductor quantum dot and film on photovaitlic and photoelectronic devices.

Dianxing Ju is currently studying for the M.S. degree in the Department of Material Science and Engineering, University of Jinan, China. Now his research interests focus on the nanostructured materials for the gas sensor applications.

Bingqiang Cao is a Taishan Scholar Professor for material physics with University of Jinan. His research group focuses on semiconducting oxide thin films, heterostructures, nanostructures, and related devices.